The Astrophysical Journal Letters, 749:L20 (5pp), 2012 April 20 doi:10.1088/2041-8205/749/2/L20

FIRST SCIENCE RESULTS FROM SOFIA/FORCAST: SUPER-RESOLUTION IMAGING OF THE S140 CLUSTER AT 37 μm

Paul M. Harvey[1], Joseph D. Adams[2], Terry L. Herter[2], George Gull[2], Justin Schoenwald[2], Luke D. Keller[3], James M. De Buizer[4], William Vacca[4], William Reach[4], and E. E. Becklin[4,5]

[1] Astronomy Department, University of Texas at Austin, 1 University Station C1400, Austin, TX 78712-0259, USA; pmh@astro.as.utexas.edu
[2] Center for Radiophysics and Space Research, Space Science Building, Cornell University, Ithaca, NY 14853, USA; jdadams@astro.cornell.edu, tlh10@cornell.edu, geg3@cornell.edu, jps10@cornell.edu
[3] Department of Physics, Ithaca College, 264 Ctr for Natural Sciences, Ithaca, NY 14850, USA; lkeller@ithaca.edu
[4] SOFIA-University Space Research Association, NASA Ames Research Center, Mail Stop N211-3, Moffett Field, CA 94035, USA; jdebuizer@sofia.usra.edu, wvacca@sofia.usra.edu, wreach@sofia.usra.edu, ebecklin@sofia.usra.edu
[5] Department of Physics and Astronomy, University of California Los Angeles, 405 Hilgard Ave., Los Angeles, CA 90095-1562, USA; ebecklin@sofia.usra.edu
Received 2011 December 28; accepted 2012 February 2; published 2012 March 29

ABSTRACT

We present 37 μm imaging of the S140 complex of infrared sources centered on IRS1 made with the FORCAST camera on SOFIA. These observations are the longest wavelength imaging to resolve clearly the three main sources seen at shorter wavelengths, IRS 1, 2, and 3, and are nearly at the diffraction limit of the 2.5 m telescope. We also obtained a small number of images at 11 and 31 μm that are useful for flux measurement. Our images cover the area of several strong submillimeter sources seen in the area—SMM 1, 2, and 3—that are not coincident with any mid-infrared sources and are not visible in our longer wavelength imaging either. Our new observations confirm previous estimates of the relative dust optical depth and source luminosity for the components in this likely cluster of early B stars. We also investigate the use of super-resolution to go beyond the basic diffraction limit in imaging on SOFIA and find that the van Cittert algorithm, together with the "multi-resolution" technique, provides excellent results.

Key words: infrared: general – ISM: individual objects (S140) – stars: formation

1. INTRODUCTION

Sharpless 140 is a relatively diffuse H II region at the edge of the much denser L1204 molecular cloud that harbors several clusters of young B stars at a distance of about 900 pc (Crampton & Fisher 1974). The most luminous object in this cloud was first observed in the near- and mid-infrared by Blair et al. (1978) and by Harvey et al. (1978) in the far-infrared. Blair et al. found a very red, compact object with a spectral energy distribution (SED) similar to that of the BN object in Orion in addition to several other less remarkable infrared sources. Using the Kuiper Airborne Observatory (KAO), Harvey et al. found strong, nearly spatially unresolved emission in the far-infrared from 35 to 175 μm. They fit several crude models to the SED that showed that the dust optical depth to the central source had to approach unity in the 50–100 μm spectral region and that the total luminosity was equivalent to that of an early B star.

In the intervening years, a host of much higher angular resolution near-infrared and radio observations have been published. These have revealed many additional infrared sources likely to be young stars or protostars as well as energetic outflows similar to those found in many other molecular clouds harboring young stars (e.g., Evans et al. 1989; Kraemer et al. 2001; de Wit et al. 2009; Preibisch & Smith 2002; Kurtz et al. 1999; Bally et al. 2002). It also seems likely that one or more of the strong mid-IR sources contain two or more young B stars (Preibisch & Smith 2002; Preibisch et al. 2001) and that the radio jet from IRS1 is likely to be due to an ionized equatorial wind (Hoare 2006). Very cold, dense condensations only emitting longward of $\lambda \sim 300\,\mu$m are also seen and may be even younger stages of star formation within the molecular cloud (Minchin et al. 1995).

Most of the luminosity of very young stellar objects and protostars is emitted in the far-infrared, wavelengths that are essentially invisible to ground-based telescopes due to absorption by water vapor. Until the recent commissioning of the *Herschel Space Observatory* (Pilbratt et al. 2010) and the Stratospheric Observatory for Infrared Astronomy (SOFIA; Gehrz et al. 2011), the far-infrared, however, has suffered from a substantial deficit in angular resolution compared to neighboring wavelengths observable with large ground-based telescopes. High mass young stars typically form in dense clusters, and this puts a special premium on the value of high angular resolution to resolve individual components to understand their evolutionary state.

We present here the first imaging observations of the S140 cluster at wavelengths longward of the ground-based atmospheric window at $\lambda \sim 20$–$25\,\mu$m with an angular resolution of a few arcseconds. With this resolution we are able to distinguish the three main luminosity sources seen at shorter wavelengths as well as diffuse emission between the objects. We describe the observations in Section 2 and then in Section 3 describe some efforts to improve the angular resolution with various deconvolution techniques. In Section 4, we compare our 31 and 37 μm maps with those at shorter and longer wavelengths and show the SEDs for the individual members of this cluster, and in Section 5 we summarize our results.

2. OBSERVATIONS AND DATA REDUCTION

Our observations were made with the FORCAST camera (Herter et al. 2012) on board SOFIA on the night of UT 2010 December 1. The FORCAST camera has two separate 256 × 256 infrared arrays that cover the wavelength range from ~5–40 μm in a variety of bands with 0.″768 × 0.″768 pixels. The two arrays can observe simultaneously through a dichroic beam splitter that divides the wavelength range shortward and longward of 26 μm, or the long wavelength array can be used by itself without

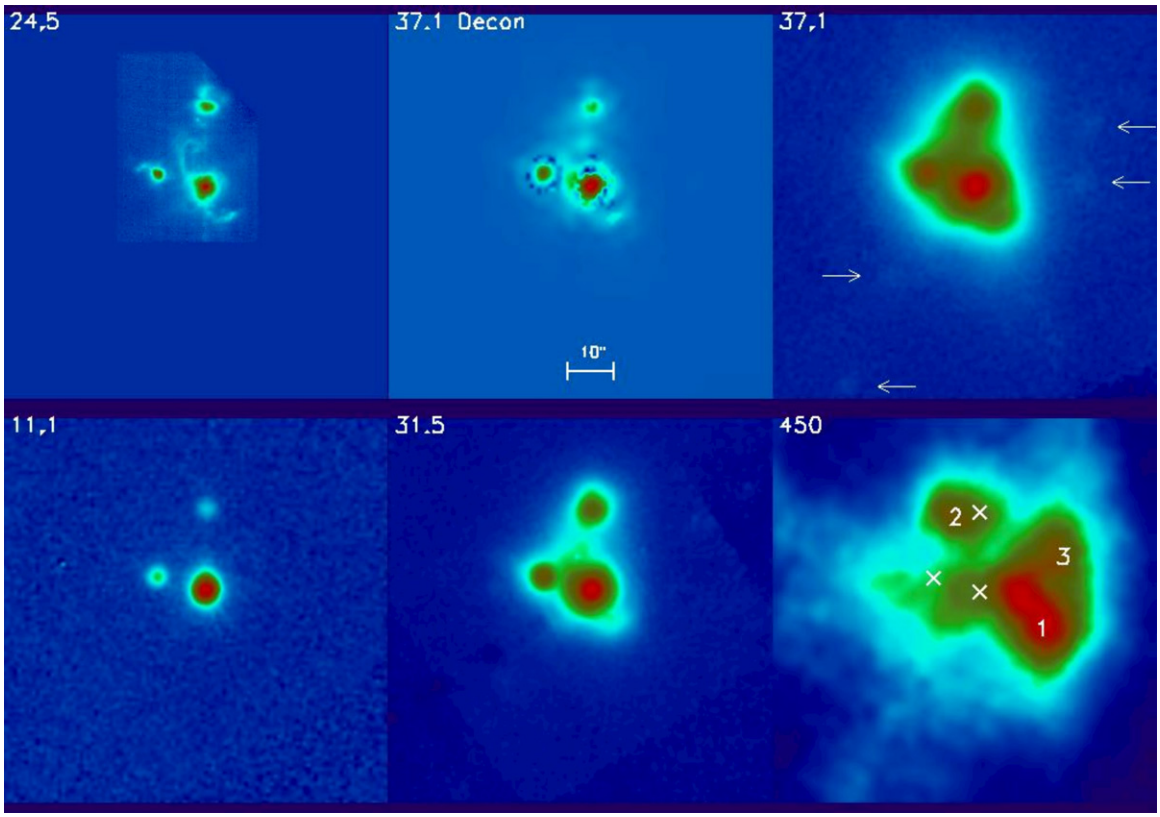

Figure 1. Top row (left to right): 24.5 μm Subaru image of de Wit et al. (2009), deconvolved 37 μm image from this paper, and observed 37 μm image from this paper; Bottom row (left to right): observed 11 μm and 31 μm images from this paper, and 450 μm images from the SCUBA archive (http://cadcwww.dao.nrc.ca/jcmt/search/product) with the positions of IRS 1, 2, and 3 marked with "X," as well as the positions of the submillimeter peaks SMM 1–3. North is up and east to the left. The locations of four faint sources that are coincident with *Spitzer* IRAC sources are indicated by arrows in the upper right panel.

the intervening dichroic. The observations presented here were made with the 37.1 μm filter (hereafter 37 μm) without the beam splitter and at 11.1 and 31.5 μm with the beam splitter (hereafter "11" and "31" μm).

In addition to the observations of S140, a number of other science investigations were undertaken that are also reported in this issue, and several calibration targets were observed for both flux and point-source-response (PSF) calibration. The FORCAST images were calibrated to a flux density per pixel using a standard instrument response derived from measurements of standard stars and solar system objects over several flights (Herter et al. 2012). The color correction from a flat spectrum source to that of S140 is negligible (<1%). The estimated 3σ uncertainty in the calibration due to variations in flat field, water vapor burden, and altitude is approximately ±20%. The PSF has been derived from averages over several flights as described in detail by De Buizer et al. (2012). We discuss below the relatively minor uncertainties involved in using this average PSF, and tests of its applicability using μ Cep data taken on the same flight as S140. The nominal diffraction limit of SOFIA at 37 μm, 1.019λ/D with its 14% central obscuration, is 3.″1, and our observations show that achieved resolution is quite close to this limit, ∼4″ FWHM. At shorter wavelengths the SOFIA PSF is affected more by telescope pointing jitter and seeing, with seeing being dominant shortward of 5 μm because of the shear layer just above the telescope (Erickson & Dunham 2000).

Our images of both S140 and μ Cep were obtained with standard thermal infrared techniques of chopping and nodding. Because the cluster is relatively compact, we were able to chop and nod completely on the ∼200 arcsec square array. The chop frequency used was 2 Hz, and chop amplitude of 90″ with a nod amplitude also of 90″ perpendicular to the chop direction. Each observation resulted in 120 s of on-chip integration as the result of one ABBA nod pair. We obtained 10 useful observations of S140 and two of μ Cep at 37 μm, and two of S140 at 11 and 31 μm. The individual observations were co-added by cross-correlating all the subsequent images with the first. The sky rotation was essentially negligible between the individual S140 observations. The telescope software to enable accurate absolute pointing was not yet operational for these observations, so we used the highest resolution, nearest wavelength observations (24.5 μm) from a large ground-based telescope (de Wit et al. 2009) to establish the absolute coordinate system for our observations. For the purposes of deconvolution discussed later, the S140 frames were left in the original instrument coordinate system to match those of the PSF calibration image.

Figure 1 shows the results of the processing described so far for S140 as well as related images from the literature discussed below. Using aperture photometry we have derived flux densities for the three obvious components of the image as well as for two additional local flux maxima. These results are listed later in Table 1 for a 9″ diameter aperture. We discuss these further in Section 4 after we describe our deconvolution work and the resulting higher resolution image. The statistical uncertainties in these fluxes are negligible because of the very high signal-to-noise ratio (S/N), well over 100, for all the sources except for the faintest objects at 11 μm where S/N ∼ 10. Table 1 also lists the luminosities of these "objects" for the assumed distance of 960 pc, using the 50–100 μm flux densities of Lester et al. (1986).

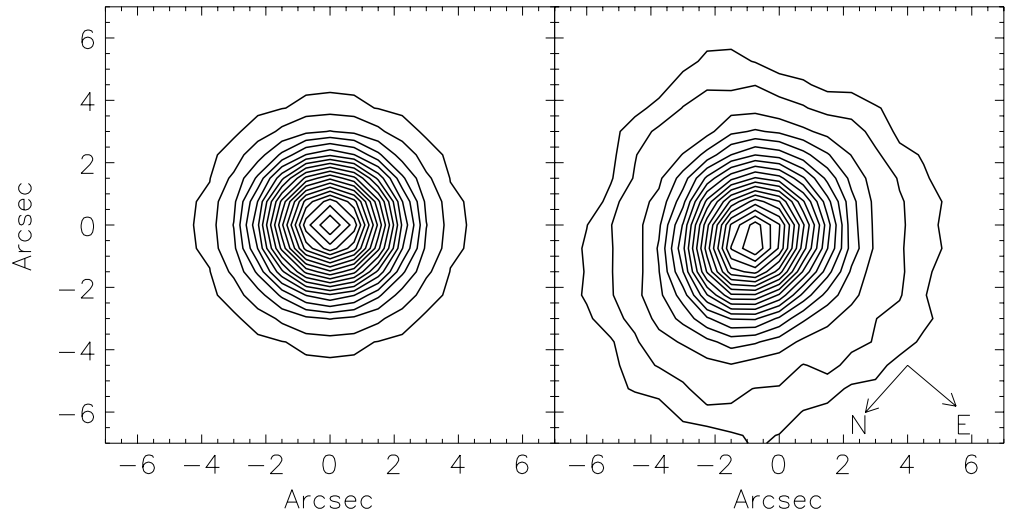

Figure 2. Left: derived PSF as described in the text. Contours are at levels of 2.5%, 5%, 10%, 15%, ..., 90%, and 95% of the peak. Right: observed image of the nominal PSF calibrator, μ Cep, with contours at the same level.

Table 1
Aperture[a] Flux Densities[b] (Jy) of Sources in S140

Image	IRS 1	IRS 2	IRS 3	NW	VLA 4	Total[c]
Observed 37 μm	2176	485	669	465	381	6730
Deconvolved 37 μm	2624	577	710	438	358	6730
Observed 11 μm	110	4.0	9.7	3.5	2.6	145
Observed 31 μm	1585	368	401	242	184	3780
Luminosity ($L_\odot$)	10,700	3200	2900	800	650	19,150

Notes.
[a] For 9″ diameter aperture.
[b] Absolute calibration uncertainty = 20%; negligible statistical uncertainty.
[c] Summed over entire map shown in Figure 1.

3. DECONVOLUTION AND SUPER-RESOLUTION

With NASA's previous airborne observatory, the KAO, Lester et al. (1986) for example showed that significant improvements in the apparent angular resolution in far-infrared images were possible through super-resolution techniques such as maximum entropy deconvolution. With the KAO's instrumentation these techniques were limited to one-dimensional scans rather than two-dimensional images. In the intervening years, the improvement in detectors and in analysis techniques suggests the possibility of substantial resolution improvements in two-dimensional far-infrared images with SOFIA. To that end we have experimented with a variety of algorithms and parameters available as part of the "MRA" package (Starck et al. 2002; Pantin & Starck 1995) to improve the resolution in our S140 image. Our best results were obtained using the van-Cittert algorithm with multi-resolution support for regularization. With this mode the final deconvolved images did not depend strongly on the number of iterations, and therefore this was used for all our results below. For example, the final image shown used 500 iterations, but the image changed very modestly after as few as 20 iterations. Additionally, we did not force positivity in the image.

As mentioned above we have used the PSF derived by De Buizer et al. (2012) and done several tests to give us confidence in its applicability to the S140 images. First, we deconvolved the observed μ Cep image and compared the result with the much higher angular resolution, but shorter wavelength 24.5 μm image of de Wit et al. (2008). We found the spatial extent and spatial asymmetry to be very similar. We also found the amplitude of the wings to the northeast and southwest to be relatively larger at 37 μm, which is entirely consistent with the expected dust temperature of order 150 K at a radius of a few arcseconds. In a second test of our derived PSF, we produced several similar PSFs with small changes in the width in both telescope axes, elevation and cross elevation, and then deconvolved the S140 image with these modified PSFs. In all cases the major details of the deconvolved images were

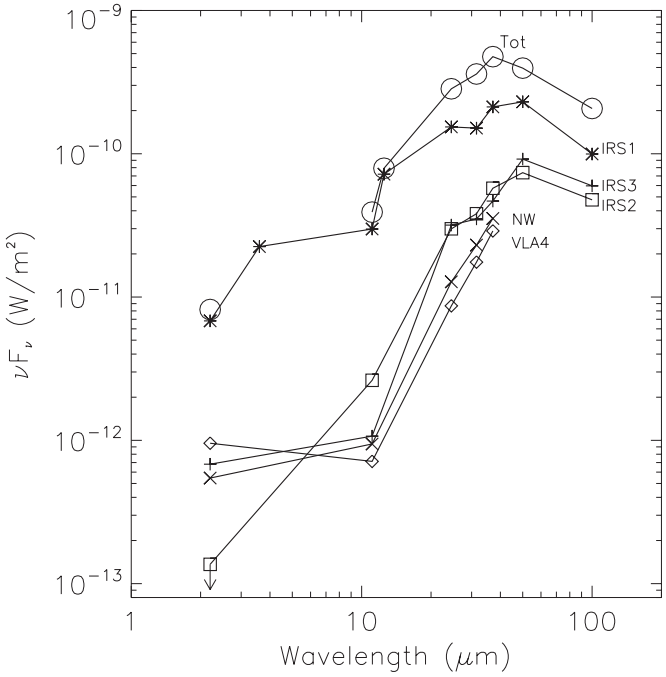

Figure 3. Spectral energy distributions of the various sources detected in the S140 region at 37 μm. For the 37 μm flux densities we have used the 9″ aperture fluxes listed in Table 1 from the deconvolved map. For the 11 and 31 μm fluxes from this study, we used the 9″ aperture fluxes in Table 1 from the observed images. At the shorter wavelengths we have used the 9″ aperture fluxes from Evans et al. (1989) at 1–2.5 μm, the 3.45 μm flux for IRS1 from Blair et al. (1978), and measured 9″ aperture fluxes from the 24.5 μm map of de Wit et al. (2009). At 50 and 100 μm we used the fluxes estimated by Lester et al. (1986) for the three major sources.

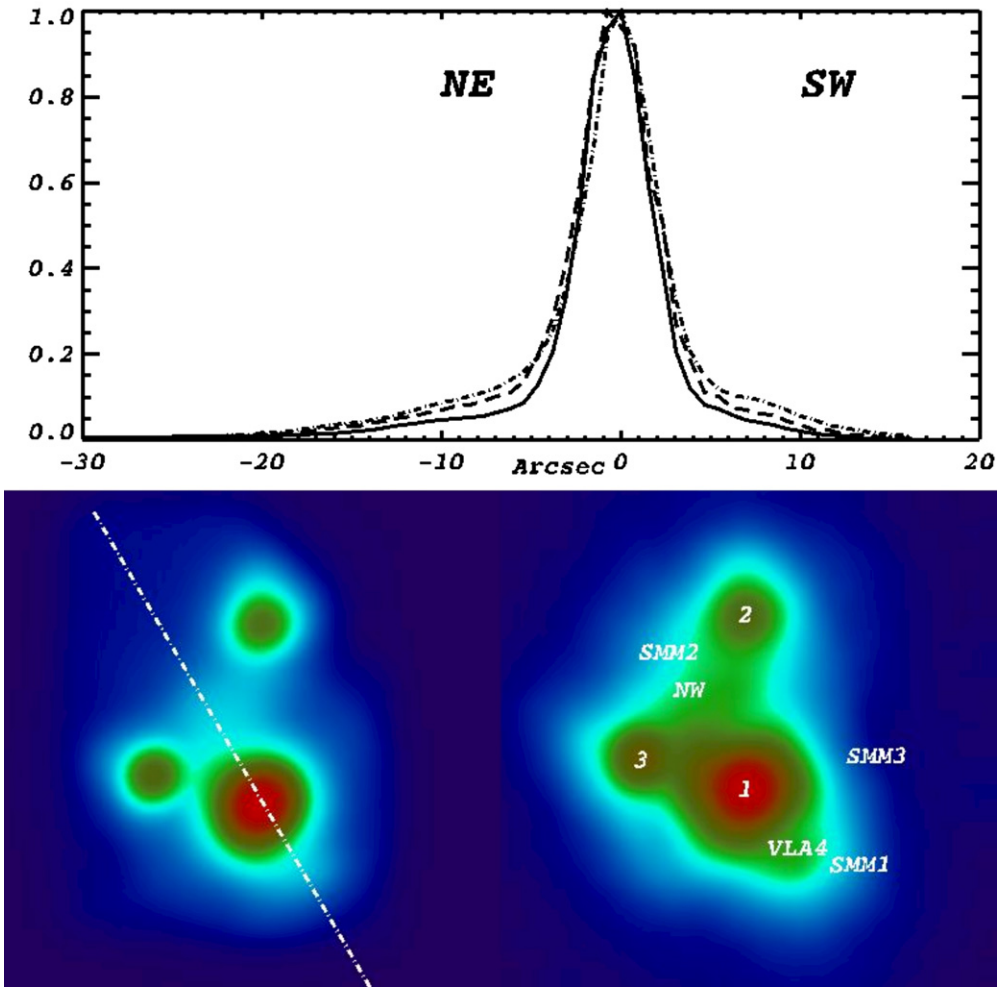

Figure 4. Bottom panel: 24.5 μm image of de Wit et al. (2009) convolved with 37 μm PSF (left), and our observed 37 μm image illustrating the more extended, diffuse emission at the longer wavelength. The diagonal line through IRS 1 marks the one-dimensional cut along which the relative fluxes are shown in the upper panel, showing quantitatively the higher level of extended emission at the longer wavelengths. The approximate positions of all the components of this source mentioned in the text are indicated in the lower right panel. Upper panel: relative fluxes along the diagonal line below for the observed 37 μm image (dash-dotted), the observed 31 μm imaged convolved to the 37 μm resolution (dash), and the 24.5 μm image of de Wit et al. (2009) convolved to the 37 μm resolution (solid).

essentially the same as for the derived PSF. So we are confident that none of our conclusions depends on the small uncertainties in our knowledge of the PSF. Finally, Figure 1 shows the observed and deconvolved images of S140 at 37 μm together with the observed Subaru image (de Wit et al. 2009). It is clear that virtually all the structure seen at the 0.″6 diffraction limit of Subaru at 24.5 μm is also visible at 37 μm in the deconvolved image, albeit at somewhat lower resolution. With the native 37 μm resolution of $\sim$4″, however, much of this structure is smoothed to the point of being barely detectable. The final derived PSF is equivalent to the theoretical diffraction-limited PSF convolved with a Gaussian of roughly 1.″5 FWHM, and the apparent resolution of the deconvolved S140 image is $\sim$2.″4. Figure 2 shows the derived PSF along with the observed μ Cep image illustrating the larger extent of μ Cep at 37 μm.

4. COMPARISON WITH GROUND-BASED MID-INFRARED AND RADIO OBSERVATIONS

We have already noted above the excellent agreement between our 37 μm deconvolved image and the much higher resolution 24.5 μm image of de Wit et al. (2009). In particular, in addition to the good agreement in position of the three main peaks, the agreement in morphology of the low level, diffuse emission north of IRS 1 and also to the southwest suggests that the deconvolution process has not developed spurious features as might have been the case with a poor estimate for the PSF or a poor algorithm. There are probably still some residual positional problems in our 37 μm image at the level of $\sim$1″ due to the inherent uncertainties in fixing the absolute positions by registering to the shorter wavelength ground-based images, but the agreement between the two images is remarkably satisfying. As a corollary it is also clear that there are no new sources present in the 37 μm data, either raw or deconvolved, that are not present in the Subaru 24.5 μm image. Most importantly, we do not see any evidence for emission above the background from either of SMM 1, SMM 2, or SMM 3, the 450 μm sources discovered by Minchin et al. (1995). At 37 μm any emission from these sources must be below a level of $\sim$30 Jy to be invisible in our image. This confirms their likely interpretation as very cold, prestellar condensations. Four very faint sources in the 37 μm image are indicated in Figure 1 that have counterparts in the *Spitzer* IRAC images in the *Spitzer* archive, presumably low-luminosity young stellar objects.

As noted earlier, Table 1 lists flux densities derived from our 37 μm image. We list both the values measured using the

raw image, as well as from the deconvolved image. Since the deconvolution algorithm conserves flux, the total flux densities for both methods are identical, but we believe the deconvolved image provides a more realistic measurement of the flux densities in small beams required for a reasonable comparison of the relative fluxes and colors of the individual components in this region. Table 1 also lists the observed 11 and 31 μm flux densities for a 9″ aperture. Figure 3 shows the SEDs for the various local maxima that have been identified previously in this region and which are clearly detected in our deconvolved map. This shows graphically the fact, as noted by previous investigators, that the coldest mid-infrared condensations in this region are the diffuse local flux maxima called "NW" and "VLA 4" (labeled in Figure 4), while the hottest SED belongs to IRS 1. IRS 2 and 3 exhibit SEDs that are intermediate in color temperature with IRS 3 being the cooler source. Quantitatively, IRS 1 dominates the shorter wavelength emission with 75% of the total emission at 11 μm, but at 37 μm it contributes less than 40% with the rest arising from the cooler sources, IRS 2, 3, NW, VLA4, and the surrounding diffuse emission.

In their original KAO study of S140 Harvey et al. (1978) showed that the dust optical depth was likely close to unity in the far-infrared based on the resolving power possible with that instrumentation. With the substantially higher spatial resolution available with SOFIA/FORCAST we can re-examine this conclusion. For example, the ratio of 37 μm to 53 μm flux densities shown in Figure 3 for IRS1 implies a color temperature of order 85 K. If we assume that half of the total flux arises in the central 4″ core, this implies $\tau \sim 0.5$ at 53 μm, quite consistent with the original KAO study.

In order to compare quantitatively the diffuse emission in our 37 μm map with that seen at much higher angular resolution at 24.5 μm by de Wit et al. (2009), it is necessary to compare the two images at identical levels of resolution. This technique was described as "beam matching" by Lester et al. (1986). Since the native resolution at 37 μm is more than a factor of 10 worse than that at 24.5 μm it is sufficiently accurate to simply convolve the 24.5 μm image with the 37 μm PSF. Figure 4 shows the original, undeconvolved 37 μm SOFIA image together with the 24.5 μm image of de Wit et al. (2009) smoothed to what would have been observed with our 37 μm SOFIA PSF. This shows that there is substantially less extended diffuse emission at 24.5 μm. Figure 4 also shows the relative 24.5, 31, and 37 μm fluxes along a one-dimensional cut through IRS 1 from northeast to southwest along the line shown in the figure. This comparison shows quantitatively the higher level of extended, diffuse emission at the longer wavelengths, consistent with a radial temperature gradient away from the center of heating. This effect can also be seen in the more steeply rising 24.5–37 μm SED slopes noted earlier for the sources labeled "NW" and "VLA4" well away from IRS1.

In order to fully model the various components of this compact cluster, it will be necessary to obtain spatially resolved images at the peaks of their SEDs, i.e., $\lambda \sim 70$ μm. For the three brightest sources, this will be possible with SOFIA using the upcoming HAWC far-IR camera. To understand the structure of the cores of the submillimeter sources would, however, require the sensitivity and higher angular resolution of *Herschel* with its PACS and SPIRE cameras.

5. SUMMARY

We have demonstrated the utility of the FORCAST camera on SOFIA for mapping compact regions of star formation at wavelengths beyond the familiar ground-based mid-IR atmospheric windows. This allows us to define the SEDs and colors of the major emission sources in S140 with unprecedented angular resolution in the far-IR. Since the data were taken with quite high S/N, we were able to successfully pursue spatial deconvolution of the image and show that the basic structure which appears at $\lambda \sim 25$ μm with subarcsecond resolution from large ground-based telescopes can also be identified in our far-IR images. We find emission from *all* the major sources seen in this cluster at shorter wavelengths from ground-based telescopes and confirm that the coolest sources are IRS3 and the diffuse knots, VLA4 and NW. We also see no evidence for emission from the submillimeter peaks in this region.

This work is based on observations made with the NASA/DLR Stratospheric Observatory for Infrared Astronomy (SOFIA). SOFIA science mission operations are conducted jointly by the Universities Space Research Association (USRA), Inc., under NASA contract NAS2-97001, and the Deutsches SOFIA Institut (DSI) under DLR contract 50 OK 0901. Financial support for FORCAST was provided to Cornell University by NASA through award 8500-98-014 issued by USRA. Support at the University of Texas was provided by USRA award 08521-012. We also especially thank W. de Wit for providing the digital versions of the 24.5 μm images for both μ Cep and S140 and acknowledge insightful comments from D. Lester and an anonymous referee. This research used the facilities of the Canadian Astronomy Data Centre operated by the National Research Council of Canada with the support of the Canadian Space Agency.

REFERENCES

Bally, J., Reipurth, B., Walawender, J., & Armund, T. 2002, AJ, 124, 2152
Blair, G. N., Evans, N. J., II, Vanden Bout, P. A., & Peters, W. L. 1978, ApJ, 219, 896
Crampton, D., & Fisher, W. A. 1974, Publ. Dom. Astrophys. Obs. Victoria, 14, 283
De Buizer, J. M., Morris, M. R., Becklin, E. E., et al. 2012, ApJ, 749, L23
de Wit, W. J., Hoare, M. G., Fujiyoshi, T., et al. 2009, A&A, 494, 157
de Wit, W. J., Oudmaijer, R. D., Fujiyoshi, T., et al. 2008, ApJ, 685, L75
Erickson, E. F., & Dunham, E. W. 2000, Proc. SPIE, 4014, 2
Evans, N. J., II, Mundy, L. G., Kutner, M. L., & DePoy, D. L. 1989, ApJ, 346, 212
Gehrz, R. D., Becklin, E. E., De Buizer, J., et al. 2011, Adv. Space Res., 48, 1004
Harvey, P. M., Campbell, M. F., & Hoffmann, F. 1978, ApJ, 219, 891
Herter, T. L., Adams, J. D., De Buizer, J. M., et al. 2012, ApJ, 749, L18
Hoare, M. G. 2006, ApJ, 649, 856
Kraemer, K. E., Jackson, J. M., Deutsch, L. K., et al. 2001, ApJ, 561, 282
Kurtz, S. E., Watson, A. M., Hofner, P., & Otte, B. 1999, ApJ, 514, 232
Lester, D. F., Harvey, P. M., Joy, M., & Ellis, H. B. 1986, ApJ, 309, 80
Minchin, N. R., Ward-Thompson, D., & White, G. J. 1995, A&A, 298, 894
Pantin, E., & Starck, J.-L. 1995, A&AS, 118, 575
Pilbratt, G. P., Riedinger, J. R., Passvogel, T., et al. 2010, A&A, 518, L1
Preibisch, T., Balega, Y. Y., Schertl, D., et al. 2001, A&A, 378, 539
Preibisch, T., & Smith, M. D. 2002, A&A, 383, 540
Starck, J. L., Pantin, E., & Murtagh, F. 2002, PASP, 114, 1051